Surface & Coatings Technology 488 (2024) 130941

Contents lists available at ScienceDirect

Surface & Coatings Technology

journal homepage: www.elsevier.com/locate/surfcoat

Tailored high-temperature corrosion behavior of Cr coatings using high power impulse magnetron sputtering on ZIRLO alloys for accident-tolerant fuel application

Zhichao Han [a,b], Zheng Wang [b], Zhenyu Wang [b,**], Shiyao Tan [b], Aiying Wang [b,c], Zhongyu Piao [a], Peiling Ke [b,c,*]

[a] College of Mechanical Engineering, Zhejiang University of Technology, Hangzhou 310014, China
[b] Key Laboratory of Advanced Marine Materials, Ningbo Institute of Materials Technology and Engineering, Chinese Academy of Sciences, Ningbo 315201, China
[c] Center of Materials Science and Optoelectronics Engineering, University of Chinese Academy of Sciences, Beijing 100049, China

ARTICLE INFO

Keywords:
Cr coatings
HiPIMS
Synchronized pulse bias
High temperature steam oxidation

ABSTRACT

To further enhance the oxidation resistance of Zirconium alloys during Loss of Coolant Accident (LOCA), protective Cr coatings were deposited in synchronized pulse bias mode through high power impulse magnetron sputtering (HiPIMS). The results showed the weight gain of the Cr coatings with synchronized pulse bias was reduced by approximately 61.7 % compared to that of the Cr coatings without synchronized pulse bias after 90 min of steam oxidation at 1200 °C. This was mainly attributed to the formed intense (200) preferred orientation of the Cr coatings with synchronized pulse bias during deposition, accelerating the recrystallization growth of the residual Cr layer in a high-temperature steam environment, thereby reducing the rapid diffusion pathways for oxygen. Moreover, the synchronized pulse bias induced Cr grains refinement, favoring the formation of a more compact Cr_2O_3 scale, and therefore efficiently inhibiting the diffusion of external oxygen to the underlying alloy.

1. Introduction

Zirconium alloy has been widely used as a nuclear fuel cladding material due to its excellent nuclear performance, good mechanical properties, and high corrosion resistance in high-temperature aqueous solutions [1]. However, in the event of a Loss of Coolant Accident (LOCA), due to the delayed response of the emergency response system, the rapid reaction occurred between the zirconium alloy cladding and steam, result in hydrogen generation and significant heat release. This reaction may cause a hydrogen explosion and core meltdown, as demonstrated by the Fukushima nuclear accident in 2011 [2]. Based on this, the concept of accident-tolerant fuel (ATF) coatings was introduced to decelerate or even prevent the Zr-H_2O reaction [3,4]. Up to now, various materials for ATF coatings have been developed [5], including MAX phase coatings [6], FeCrAl coatings [7,8], SiC coatings [9], and Cr coatings [10–12], etc. Among these, the metal Cr coating stands out for its good corrosion resistance [13], excellent high-temperature oxidation resistance [14,15], abrasion resistance [16], and low thermal neutron absorption cross-section [17,18].

In recent years, various techniques such as cold spraying [19], plasma spraying [20,21], 3D laser [22], and physical vapor deposition (PVD) [11] have been used to deposit Cr coatings on zirconium alloys. Among these methods, the Cr coating produced by PVD technology, which includes arc ion plating (AIP), direct current magnetron sputtering (dc-MS), and high power impulse magnetron sputtering (HiPIMS), is distinguished by its thin and dense structure, making it highly compatible with the requirements for oxidation resistance of the cladding. HiPIMS technique is one of the PVD techniques that has been developed in recent years. It offers a high dissociation rate, strong binding force, and strong wrapping property, making it advantageous to prepare dense, low defects and smooth surface coatings. Research conducted by Wang et al. [11] found that the oxidation behavior of Cr coatings is primarily influenced by the microstructure and defects. When comparing Cr coatings prepared by AIP, the HiPIMS-Cr exhibits superior resistance to high-temperature oxidation at 1100 °C and 1200 °C. Zhang et al. [23] conducted a comparison of the high-temperature oxidation

* Correspondence to: P. Ke, Key Laboratory of Advanced Marine Materials, Ningbo Institute of Materials Technology and Engineering, Chinese Academy of Sciences, Ningbo 315201, China
** Corresponding author.
E-mail addresses: wangzy@nimte.ac.cn (Z. Wang), kepl@nimte.ac.cn (P. Ke).

https://doi.org/10.1016/j.surfcoat.2024.130941
Received 4 February 2024; Received in revised form 4 May 2024; Accepted 23 May 2024
Available online 24 May 2024

behavior between Cr coatings prepared by DCMS and HiPIMS. They discovered that cracks or defects resulting from grain boundary bonding during the grain growth of DCMS-Cr coatings served as diffusion channels for oxidizing media, thereby accelerating the oxidation of Cr coatings. Hence, the use of HiPIMS technology in the preparation of Cr coatings is anticipated to impart the necessary properties to the Cr coating, enabling it to serve as a protective layer for zirconium alloys under LOCA conditions.

Previous studies have demonstrated that deposition parameters, including thickness [24], temperature [25], bias voltage [14], pressure [26], and synchronized pulse bias [27], significantly influence the microstructure and properties of the films. Kuo et al. [27] discovered that the application of synchronized pulse bias can enhance the density of Cr coatings. The application of the synchronized pulse bias technique can enhance the bombardment of Cr, diminish defects and voids in the deposited coatings, and augment the hardness of the Cr coatings. Consequently, it is anticipated that Cr coatings prepared by HiPIMS with synchronized pulse bias exhibit superior properties compared to those prepared without synchronized pulse bias. This could provide enhanced protection for the zirconium alloys cladding during LOCA conditions. Despite significant attention given to the preparation method of Cr coatings, research is lacking on how the synchronized pulse bias technique affects the oxidation behavior of Cr coatings used in zirconium alloys coatings for nuclear fuel cladding.

This work aims to study the effect of synchronized pulse bias on the high-temperature steam resistance of Cr coatings. The steam oxidation resistance of the two coatings at 1200 °C was investigated by subjecting them to oxidation for 30, 60, and 90 min at 1200 °C in a steam environment. In addition, the mechanism of high-temperature steam oxidation of Cr coatings was revealed, taking into account the differences in microstructural morphology, preferential orientation and oxidation behavior of the two coatings.

2. Experimental procedure

2.1. Cr coating preparation

The preparation of Cr coatings was performed using HiPIMS with and without synchronized pulse bias. The substrate is ZIRLO alloys (15 mm × 10 mm × 2 mm), consisting of major alloying elements of Sn (0.77 at. %), Nb (0.98 at. %), Fe (0.16 at. %), and Zr (balance). Prior to the deposition, the substrates underwent sequential polishing using silicon carbide paper with grit sizes ranging from 400 to 3000. Subsequently, the substrates were cleaned ultrasonically in acetone and ethanol for 15 min.

Cr coatings were deposited onto zirconium alloys substrates using the HiPIMS technique with and without synchronized pulse bias on the homemade deposition system (Fig. 1). In order to guarantee uniformity of coating and complete coating of the sample surface with Cr, the substrates were mounted on a rotating jig plate facing the Cr target. The chamber was pumped down to a base pressure lower than 4×10^{-3} Pa and heated to 200 °C. A total of 40 ml/min of argon gas was passed through and the argon gas was introduced to a linear ion beam source, where Ar + ion precleaning was generated at a bias of −300 V to remove the contamination or oxides adherent to the substrate surface. During all deposition processes, 50 ml/min of argon was passed through, and a negative bias of −80 V was applied to the substrate. The deposit time was controlled to obtain similar coating thicknesses for each deposition method. The HiPIMS generator that we are using is the SPIK3000A from the Melec company. The parameters used for the deposition with the two techniques are listed in Table 1. Real-time monitoring of the HiPIMS sputtering cathode and synchronized pulse bias discharge waveforms was conducted using an oscilloscope, and the corresponding discharge waveforms can be observed in Fig. 2.

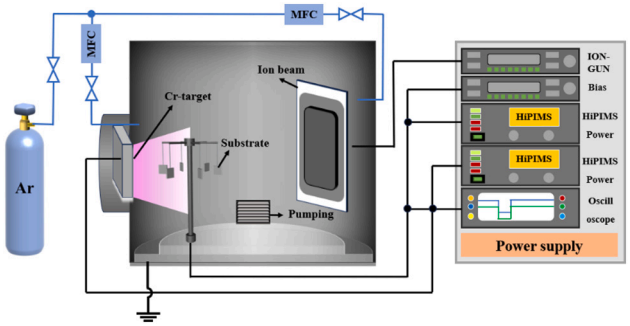

Fig. 1. Diagram of magnetron sputtering equipment.

2.2. Steam oxidation test

The steam oxidation test was conducted using an HLG-14C tube furnace and steam generator combination device. Initially, the tube furnace was heated to 600 °C, and a uniform steam flow rate of 1.5 ml/min was introduced into the furnace tube. Once the steam flow reached a stable rate, the temperature of the tube furnace was raised to 1200 °C. The samples were then positioned in the center of the furnace tube and maintained at a constant temperature for a duration of 30 min. After completing the steam oxidation test, the samples were carefully removed and allowed to cool to room temperature. The weight of each sample before and after oxidation was measured using a balance with an accuracy of 0.1 mg to determine the weight gain resulting from oxidation. To assess the effects of high-temperature steam oxidation on Cr coatings deposited through two different methods, thermogravimetric analysis (TGA) was conducted using a Netzsch instrument from Germany. The test conditions included a temperature of 1200 °C, steam with 70 % relative humidity, Ar gas as the carrier gas, and a ramp rate of 10 °C per minute, with steam introduced at a temperature of 1200 °C.

2.3. Coating performance characterization

The physical structure of the coating samples was analyzed using a D8-Advance Brucker X-ray diffractometer (XRD) with a scanning range from 10° to 90°, both before and after high-temperature steam oxidation. The XRD analysis employed the Cu Kα spectral line (wavelength λ = 0.15406 nm), with tube voltage and current set to 40 kV and 40 mA respectively. To examine the cross-sectional morphology and composition, samples of both pre- and post-steam oxidation were encapsulated in epoxy resin, polished, and analyzed using a Verios G4 Thermal Field Emission Scanning Electron Microscope (SEM) equipped with an energy-dispersive spectrometer (EDS). In addition, the samples before and after steam oxidation were ground, polished and ion beam polished, and the coating samples before and after high temperature steam oxidation were subjected to EBSD testing using a Verios G4 Thermal Field Emission Scanning Electron Microscope equipped with an EBSD probe.

3. Results

3.1. Structure and composition of coating

Fig. 3(a) shows the XRD patterns of the Cr coatings prepared by the HiPIMS with and without synchronized pulse bias. Within the scanning range of 2θ from 20° to 90°, three distinct peaks are located at 44.37°, 64.55°, and 81.69°. These peaks correspond to the crystal planes (110), (200), and (211), respectively (PDF#06–0694), within the body-centered cubic (bcc) structure of Cr. To determine the preferred orientation of the Cr coatings accurately, various crystal plane texture coefficients of the as-deposited coatings were calculated by the following formula [28]:

Table 1
Deposition parameters of the Cr coatings prepared with and without synchronized pulse bias.

Method	Time (min)	Bias			Power supply				
		Voltage (V)	Peak current (A)	Average current (A)	Power (kW)	Current (A)	Voltage (V)	Pulse width (μs)	Duty ratio
Etching	15	−300							
HiPIMS	420	80		0.24	3.0	4.0	760	100	5 %
HiPIMS with synchronized pulse bias.	420	80	10.8	0.2	3.0	4.0	760	100	5 %

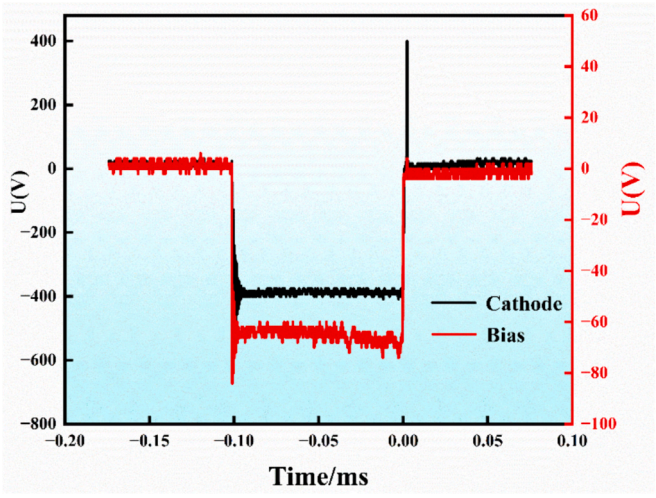

Fig. 2. Typical waveforms of the HiPIMS cathode and the synchronized pulse bias.

$$TC = \frac{I_{(hkl)}/I_{0(hkl)}}{\sum\left[I_{(hkl)}/I_{0(hkl)}\right]}$$

where $I_{(hkl)}$ is the diffraction intensity of the Cr coatings sample at the (*hkl*) crystal plane, $I_{0(hkl)}$ is the diffraction intensity of the standard unselectively oriented sample at the (*hkl*) crystal plane, and TC is the texturing coefficient. Fig. 3(b) presents the specific texture coefficient results for the two Cr coatings. Generally, higher texture coefficient values indicate a stronger preferred phase orientation within the crystals. Surprisingly, both coatings exhibited a (200) preferred orientation. However, the Cr coating prepared with synchronized pulse bias displayed a predominantly (200) preferred orientation on its surface. This observation suggests that synchronized pulse bias promotes the increase of (200) preferred orientation. The (110) crystal planes of bcc-Cr coatings possess lower surface energy, while the (200) crystal planes exhibit higher surface energy [29]. The synchronized pulse bias, in conjunction with the efficient alignment of the accelerated bias waveform and the HiPIMS pulse discharge waveform from the sputtering cathode, achieves a selective energizing effect on the ions of sputtering materials. This enhancement in ion energy contributes to the improved energy of the coating, promoting growth on the (200) crystalline surfaces that possess higher surface energy.

This paragraph addresses the surface morphology and cross-sectional morphology of Cr coatings obtained through HiPIMS with and without synchronized pulse bias. Fig. 4 illustrates the differences in surface and cross-sectional morphology between the two coating techniques. Fig. 4 (c) and (f) demonstrates that the thickness of the Cr coatings without and with synchronized pulse bias measures 10.75 μm and 10.77 μm, respectively. The marginal disparity in thickness results from variations in deposition rates. The slight variation in thickness can be attributed to the difference in deposition rates, which are calculated to be 1.536 μm/h and 1.538 μm/h for Cr coatings without and with synchronized pulse bias, respectively. The finding indicated that the synchronized pulse bias has minimal impact on the coatings' deposition rate. As shown in Fig. 4 (a) and (d), both coating surfaces exhibited uniform density without noticeable cracks. However, when the coating thickness was held constant, the Cr coating prepared using synchronized pulse bias displayed a more uniform and denser surface. For the Cr coatings prepared without synchronized pulse bias, there are significant differences between the grains, with a large number of irregular blocky structures and small grains on the coating surface, and the grains are not uniformly distributed. However, the application of synchronized pulse bias reduces the pronounced disparity between grains. Simultaneously, dense grains are uniformly distributed on the surface of the Cr coatings prepared using synchronized pulse bias as shown in Fig. 4(b) and (e). This improvement can be attributed to the synchronized pulse bias, which effectively matches the acceleration bias waveform with the pulsed discharge waveform of the sputtering cathode in HiPIMS. Consequently, this technique, through the strategic application of synchronized pulse bias, enables the selective enhancement of the energy of sputtered Cr ions. This selective energization facilitates their accelerated deposition onto the substrate surface. By increasing the kinetic energy of Cr ions, the technique significantly increases the surface nucleation rate during coating growth and effectively fills grain boundaries, resulting in the deposition of dense Cr coatings.

To further determine the effect of synchronized pulse bias on the microstructure of the Cr coating, we performed EBSD characterization. The EBSD characterization of Cr coatings obtained through HiPIMS without synchronized pulse bias is introduced in this paragraph. Fig. 5

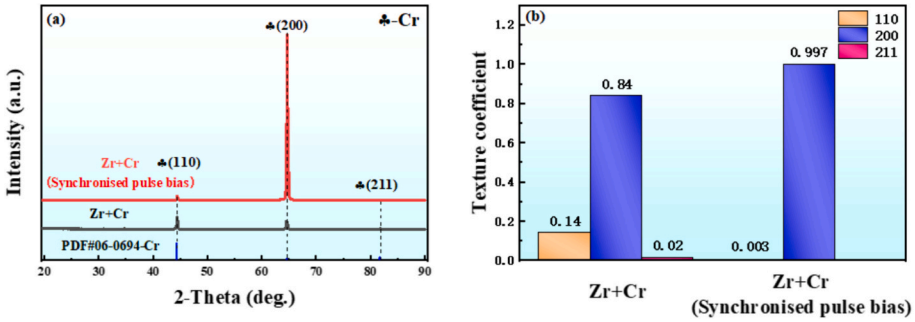

Fig. 3. XRD spectra (a) and texture coefficients (b) of the Cr coatings prepared by HiPIMS with and without synchronized pulse bias.

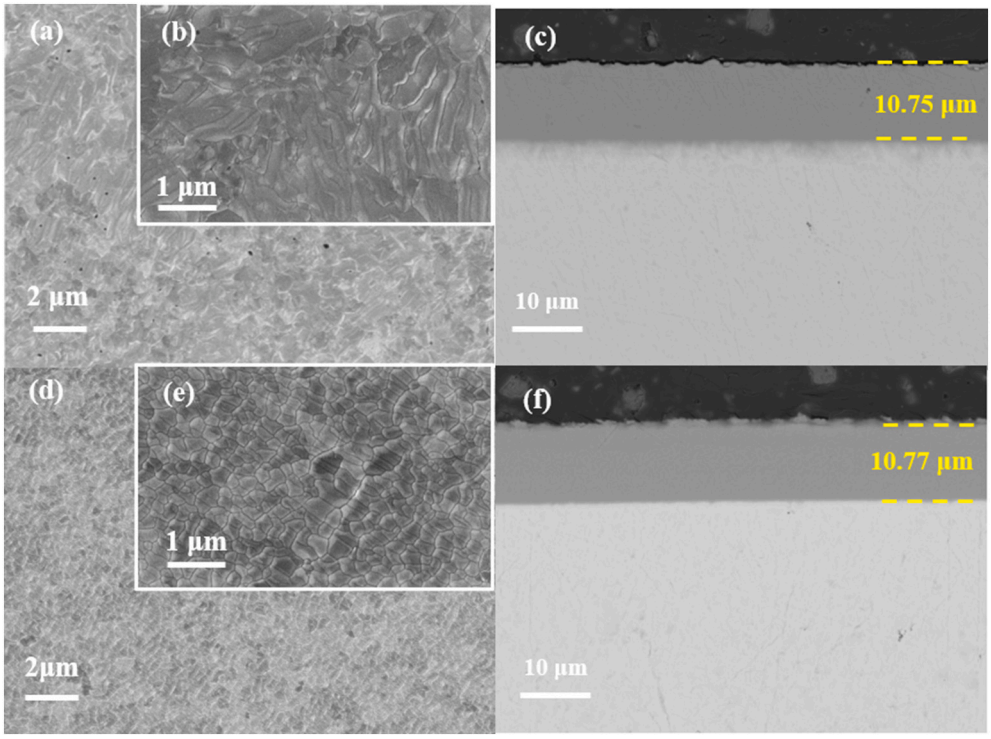

Fig. 4. Surface morphology (a), (b) and cross-sectional morphology (c) of the Cr coatings prepared by HiPIMS, Surface morphology (d), (e) and cross-sectional morphology (f) of the Cr coatings prepared by HiPIMS with synchronized pulse bias.

presents the IPFy images Fig. 5(a), the phase image Fig. 5(b), and PFs of {110}, {200}, and {211} planes Fig. 5(c). The phase image Fig. 5(b) reveals the columnar crystal growth structure of the Cr coating, indicating a uniform and dense deposition. The PF analysis Fig. 5(c) demonstrates a {200} texture in the Cr coating, while the distribution of texture in {110} and {211} planes appear to be scattered, indicating that the Cr coatings prepared without synchronized pulse bias is (200) preferred orientation. The IPFy images in Fig. 5(a) reveal that the Cr coatings prepared by HiPIMS predominantly consist of columnar grains.

This paragraph introduces the EBSD characterization of Cr coatings obtained through HiPIMS with synchronized pulse bias. Fig. 6 presents the IPFy images Fig. 6(a), the phase image Fig. 6(b), and PFs of {110}, {200}, and {211} planes Fig. 6(c). The phase image Fig. 6(b) demonstrates that Cr coatings prepared with synchronized pulse bias disrupt the columnar crystalline growth, resulting in a dense coating deposition. The PF analysis reveals a {200} texture in the Cr coating, while the distribution of texture in {110} and {211} planes appear to be scattered. The use of synchronized pulse bias leads to higher texture intensity in the (200) direction, indicating a strong preferred orientation, consistent with the XRD patterns and texture coefficient results. In addition, the XRD test provides macro-orientation, while the EBSD test offers micro-orientation. The compatibility between macro-orientation and micro-

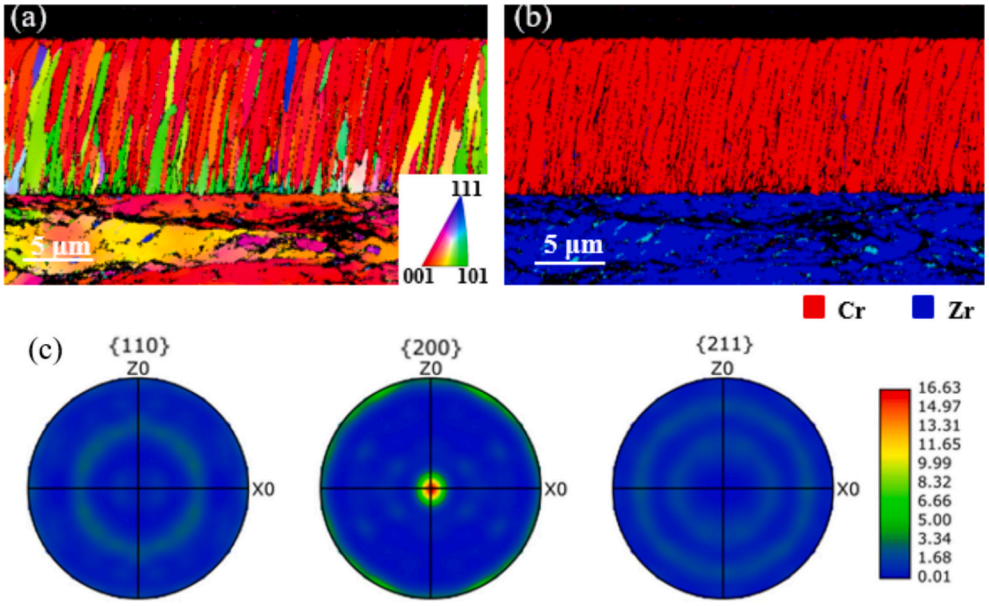

Fig. 5. EBSD maps of the Cr (HiPIMS without synchronized pulse bias) coated ZIRLO alloys: (a) IPFy map, (b) phase map, (c) PF diagram of Cr coating.

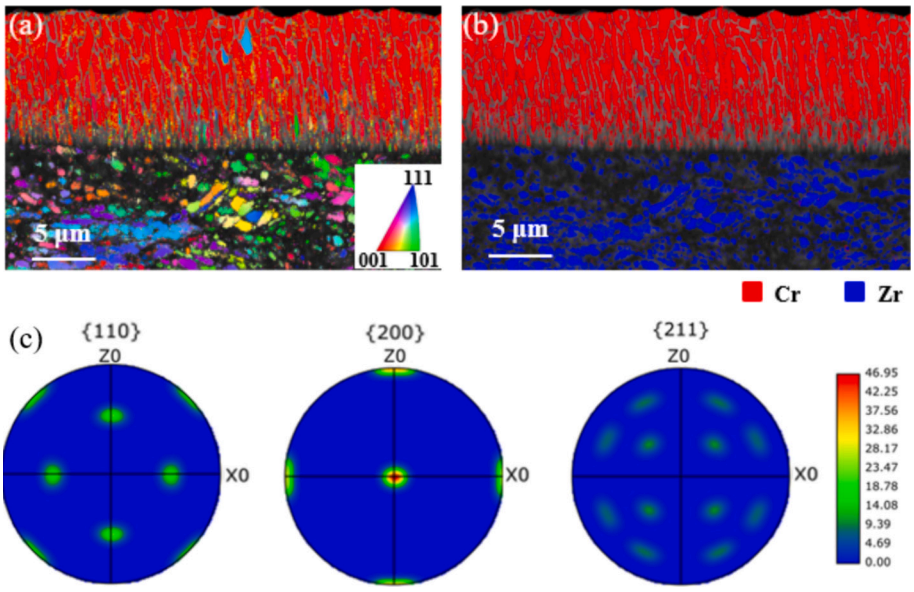

Fig. 6. EBSD maps of Cr (HiPIMS with synchronized pulse bias) coated ZIRLO alloys: (a) IPFy map, (b) phase map, (c) PF diagram of Cr coating.

orientation ensures the data's authenticity and reliability. The IPFy images Fig. 6(a) show that the synchronized pulse bias interrupted the growth of columnar crystals and the coatings had unequal grain sizes, which tended to increase from the Cr/Zr interface to the coating surface. Notably, Cr coatings prepared with synchronized pulse bias exhibit a thin layer near the coating-substrate interface, comprising nanoscale microcrystals. These microcrystals potentially serve as nucleation sites during the early stages of deposition. This is mainly due to the fact that the synchronized pulse bias enables the accelerating bias waveform to effectively match with the sputtering cathode HiPIMS pulsed-discharge waveform and achieves a selective energizing effect on the ions of sputtering materials. The high-density ions are accelerated to reach the film-forming surface, which significantly improves the nucleation rate of the coating growth surface. And the disruption of columnar crystal growth is likely attributable to the bombardment of high-energy Cr ions.

3.2. Oxidation properties of Cr coatings

3.2.1. Oxidation at 1200 °C for 30 min

Fig. 7 displays the surface morphology of Cr coatings prepared by HiPIMS with and without synchronized pulse bias after being subjected to steam oxidation at 1200 °C for 30 min. As shown in Fig. 7(b) and (d), the surfaces of both coatings are smooth and flat, displaying a distinct oxidized morphology characterized by the presence of short rod-shaped protrusions. A previous study [11] showed that such protrusions are Cr_2O_3 grains. Such protrusions have a relationship with the thermal stress and microstructure evolution of the Cr_2O_3 oxide layer during the steam oxidation [30]. Figs. 5(a) and 6(a) demonstrate that the implementation of synchronized pulse bias interrupts the growth of columnar crystals in the Cr coatings, leading to the formation of a greater number of grain boundaries. Moreover, as shown in Fig. 7(a) and (c), the Cr coating prepared with synchronized pulse bias shows significantly fewer short rod-shaped protrusions compared to the Cr coating without synchronized pulse bias. This decrease can probably be ascribed to the heightened presence of grain boundaries in the Cr coating prepared with synchronized pulse bias, which allows for a better release of thermal stresses during the oxidation process, thus inhibiting the expansion of Cr_2O_3 grains and the spillover from grain boundaries during the oxidation of chromium atoms to Cr_2O_3 in a steam environment.

Fig. 8(a) and (b) depicts the cross-sectional morphology of the two coatings following a 30-min steam oxidation at 1200 °C. An analysis of EDS line scanning results reveals that the coating samples can be categorized, from the coating surface to the substrate, into layers of Cr_2O_3, residual Cr, Zr/Cr interdiffusion. This finding suggests that the Cr coatings effectively protect the zirconium alloys in high-temperature steam corrosion for 30 min. The average thicknesses of the Cr_2O_3 layers in Cr coatings prepared with synchronized pulse bias were found to be smaller than those in Cr coatings prepared without synchronized pulse bias. Conversely, the thicknesses of Cr layers in Cr coatings prepared with synchronized pulse bias were found to be larger than those in Cr coatings prepared without synchronized pulse bias. This discrepancy in thickness can be attributed to the preferential formation of a dense

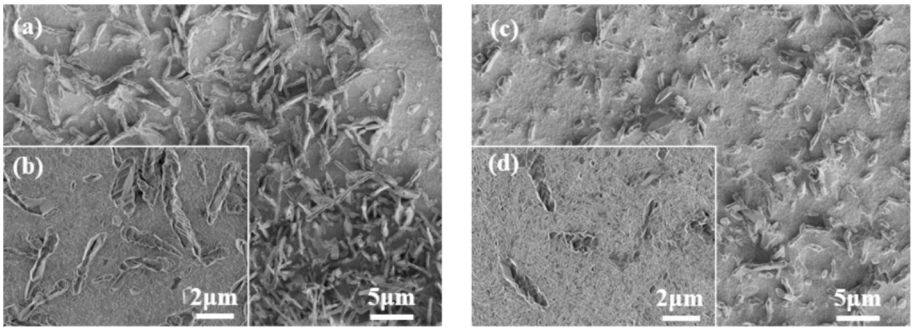

Fig. 7. SEM images of the surface morphology of the two coatings after high temperature steam corrosion (a, b) HiPIMS without synchronized pulse bias (c, d) HiPIMS with synchronized pulse bias.

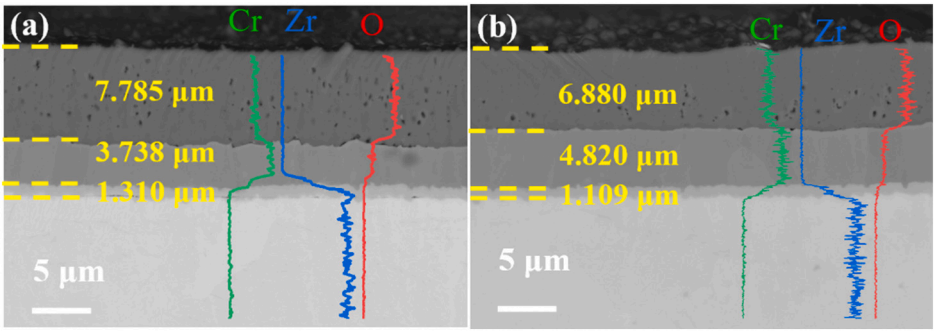

Fig. 8. Cross-section SEM images of the Cr-coated ZIRLO substrates oxidized at 1200 °C for 30 min with the corresponding EDS results (a) HiPIMS without synchronized pulse bias (b) HiPIMS with synchronized pulse bias.

Cr_2O_3 layer in coatings prepared with synchronized pulse bias. This layer inhibits steam diffusion, reducing the reaction between the Cr coatings and steam, and also mitigates the diffusion of oxygen into the substrate along the grain boundaries of the Cr coatings. Consequently, Cr coatings prepared with synchronized pulse bias exhibit superior oxidation properties following steam oxidation at 1200 °C for 30 min.

To further investigate the impact of synchronized pulse bias on the microscopic morphology of the Cr coatings, EBSD analysis was conducted on both samples. Fig. 9 shows the EBSD plots of the two coatings after steam oxidation at 1200 °C for 30 min. The initial layer consists of a Cr_2O_3 oxide film with a refined grain structure, appearing as gradient equiaxed crystals. The distinctive feature of this gradient-distributed grain microstructure is the varying density of grain boundaries, which corresponds to changes in properties. The overall properties of the coatings can be affected by sudden changes in structural size. However, the gradient structure of different sizes of grains can coordinate with each other, optimizing and improving the performance, including its corrosion behavior [31]. The gradient distribution of Cr_2O_3 grains effectively hinders the diffusion of oxygen atoms and enhances the oxidation resistance of the coatings [32–34]. Additionally, the Cr coating prepared with synchronized pulse bias exhibits smaller Cr_2O_3 grains with a more pronounced gradient distribution, resulting in improved resistance to high-temperature oxidation. In both coatings, the second layer impresses a residual Cr layer, without any noticeable preferred orientation. However, the coatings prepared with synchronized pulsed bias have a greater residual Cr layer thickness, larger grain size, and lower grain boundary fraction. Consequently, the formation of rapid oxygen diffusion channels such as ZrO_2 in the residual Cr layer was reduced. It has been demonstrated that the ZrO_2 grains present in the residual Cr layer play a significant role as the primary pathway for oxygen diffusion, which ultimately leads to the failure of the Cr coating [31,35,36]. The third layer consists of the Zr/Cr interdiffusion layer, which forms by the diffusion of Zr atoms into the Cr coating and Cr atoms into the zirconium alloys matrix at high temperatures. The fourth layer comprises a zirconium alloys matrix. The matrix is initially in the α-Zr phase before high-temperature oxidation, which then transforms to the β-Zr phase during high-temperature oxidation and subsequently to the Prior β-Zr phase upon cooling to room temperature. Consequently, both coatings demonstrate favorable resistance to high-temperature oxidation, the Cr coating prepared with synchronized pulse bias exhibits superior resistance to high-temperature oxidation.

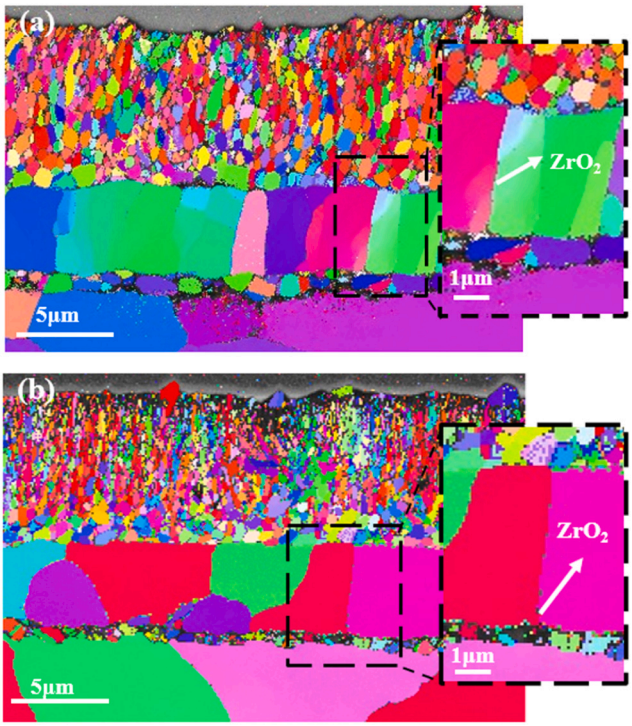

Fig. 9. EBSD plots of two coatings after steam oxidation at 1200 °C for 30 min (a) HiPIMS without synchronized pulse bias (b) HiPIMS with Synchronized pulse bias.

3.2.2. Oxidation at 1200 °C for 60 min

Fig. 10 displays the surface morphology and cross-section morphology of Cr coatings prepared by HiPIMS with and without synchronized pulse bias after being subjected to steam oxidation at 1200 °C for 60 min. As shown in Fig. 10(a) and (c), the surfaces of both coatings were smooth and flat, but bubbles appeared on the surface of the Cr coating prepared without synchronized pulse bias. Previous studies [37] have shown that the evaporation of gaseous CrO_3 and $CrO_2(OH)_2$. The number of bubbles may be related to the grain size and the number of defects in the Cr coatings. Pores were observed in the Cr_2O_3/Cr cross-section of both Cr coatings, as depicted in Fig. 10(b) and (d). This observation is consistent with the findings reported in the literature [38], where the formation mechanism was attributed to vacancy coalescence at the interface between Cr_2O_3 and Cr. Previous literature [39] also reported similar results, suggesting that the presence of pores within the Cr_2O_3 layer could be attributed to outward diffusion of Zr along the Cr grain boundaries. The thickness of both the Cr_2O_3 layer and the Cr layer in both groups of Cr-coated samples exhibited minimal variation when compared to the samples oxidized for 30 min. Based on previous literature, it is shown that a partial reduction reaction of Cr_2O_3 occurs in both Cr coatings.

To investigate the effect of the synchronized pulse bias on the oxidation characteristics of the Cr coatings, EBSD analysis was carried out on both samples. Fig. 11 shows the EBSD and EDS plots of both coatings after 60 min of steam oxidation at 1200 °C. The initial layer remains composed of gradient distributed Cr_2O_3 isocrystals, which effectively prevents the diffusion of oxygen atoms and increases the

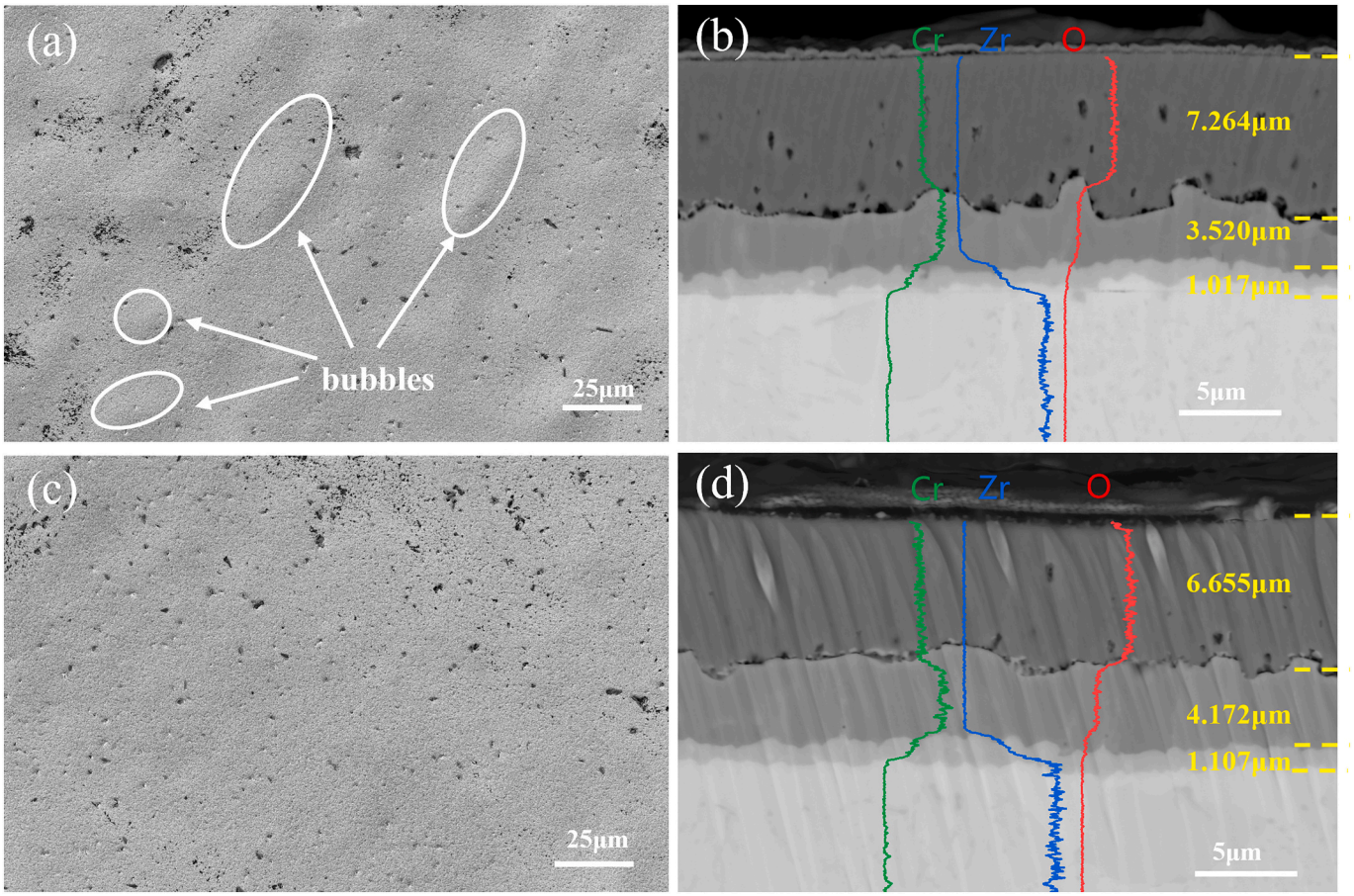

Fig. 10. Surface and cross-section SEM images of the Cr-coated ZIRLO substrates oxidized at 1200 °C for 60 min (a, b) HiPIMS without synchronized pulse bias (c, d) HiPIMS with synchronized pulse bias.

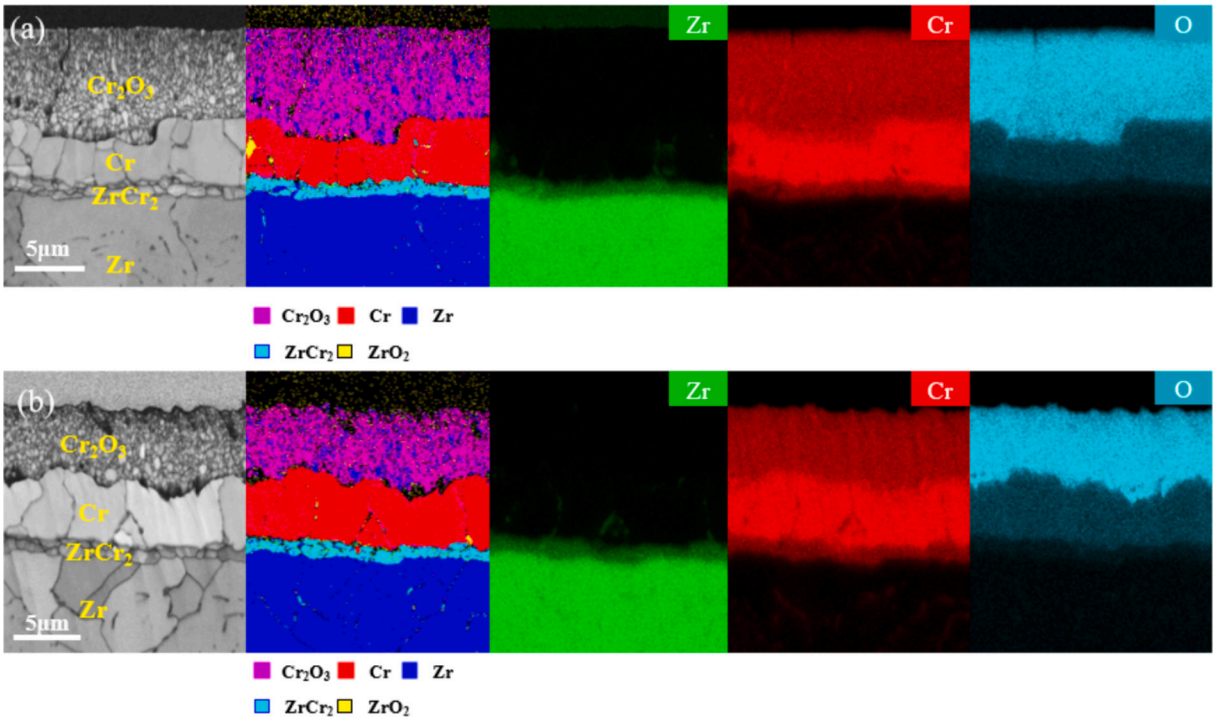

Fig. 11. EBSD plots and EDS plots of two coatings after steam oxidation at 1200 °C for 60 min (a) HiPIMS without synchronized pulse bias (b) HiPIMS with Synchronized pulse bias.

oxidation resistance of the coatings. The interface between Cr_2O_3 and Cr shows a wavy pattern, which is clearly distinguishable from the sample oxidized for 30 min. This unevenness may be due to the uneven diffusion of Zr along the Cr grain boundaries, leading to variations in the thickness of the reduced Cr layer. The EBSD and EDS plots show the presence of ZrO_2 formation along the Cr grain boundaries. In addition, the grain size of the remaining Cr layer in the Cr coating prepared with synchronized pulse bias remains larger than that prepared without synchronized pulse bias, resulting in a reduced proportion of grain boundaries and a lower amount of ZrO_2. Furthermore, based on EDS analysis, the presence of the O element is limited to the Cr_2O_3 layer and Cr, indicating that both sets of Cr coatings effectively protect the zirconium alloys against oxidation even after 60 min of high-temperature steam corrosion.

3.2.3. Oxidation at 1200 °C for 90 min

Fig. 12 displays the surface morphology and cross-section morphology of Cr coatings prepared by HiPIMS with and without synchronized pulse bias after being subjected to steam oxidation at 1200 °C for 90 min. Fig. 12(a) and (c) reveals that the surface of the Cr coatings prepared without synchronized pulse bias exhibited numerous bubbles and a few cracks. Conversely, the surface of the Cr coating prepared with synchronized pulse bias exhibited only small bubbles. Fig. 12(b) and (d) shows the Cr coatings from both groups after 90 min of steam oxidation. Compared to the samples oxidized for 30 and 60 min, the Cr layer showed increased thickness while the Cr_2O_3 layer was rapidly consumed. These results are in agreement with previous literature [10,40].

To further characterize the oxidation performance of Cr coatings after 90 min of steam corrosion, two Cr coatings were analyzed using EBSD. Fig. 13 shows the EBSD and EDS plots of the two Cr coatings after being subjected to 90 min of steam oxidation at 1200 °C. The plots reveal a significant number of ZrO_2 grains within the Cr layer of samples prepared without synchronized pulse bias. Large-sized and concentrated grains are observed at the interface between the Cr layer and the Zr/Cr interdiffusion layer. ZrO_2 grains are also detected within the Cr layer of samples prepared with synchronized pulse bias. However, their grain sizes are smaller, and they exhibit a uniform distribution along the grain boundaries of the Cr grains. Additionally, EDS observations showed that only the O element was present on the Cr_2O_3 and Cr layers, confirming that the Cr coatings effectively protected the zirconium alloy substrate even after 90 min of oxidation.

Although the microstructure of the oxidized coating can provide some insight into the coating's oxidation behavior, visually representing the oxidation process of the coating is challenging. To compare the high-temperature steam resistance of Cr coatings prepared by HiPIMS with and without synchronized pulse bias, we obtained oxidation kinetics curves for the Zr substrate, the Cr coatings without synchronized pulse bias, and the Cr coatings with synchronized pulse bias at 1200 °C for 90 min, as depicted in Fig. 14. During the initial stage of oxidation, the oxidation weight gain per unit area is higher for the Cr coatings prepared without synchronized pulse bias compared to the Cr coatings prepared with synchronized pulse bias. In addition, the difference between the weight gain per unit area of the Cr coatings prepared without synchronized pulse bias and the weight gain per unit area of the Cr coatings prepared with synchronized pulse bias gradually increased with increasing exposure time. Until after holding at 1200 °C for 90 min, the oxidative weight gain per unit area of Cr coatings prepared with synchronized pulse bias was reduced by 61.7 % compared to Cr coatings prepared without synchronized pulse bias. Fig. 14 clearly illustrates that the oxidized weight gain per unit area is significantly lower for the two samples with Cr coatings compared to the zirconium alloys matrix. Therefore, the Cr coating prepared with synchronized pulse bias was provided with excellent high-temperature oxidation resistance and can improve the safety of zirconium cladding significantly to reduce its oxidation weight gain greatly.

4. Discussion

As illustrated in Fig. 3, the preferred orientation of the Cr (200) coating is evident in those prepared with synchronized pulse bias. This orientation is attributed to the use of synchronized pulse bias, which is employed in conjunction with the effective matching of the accelerated

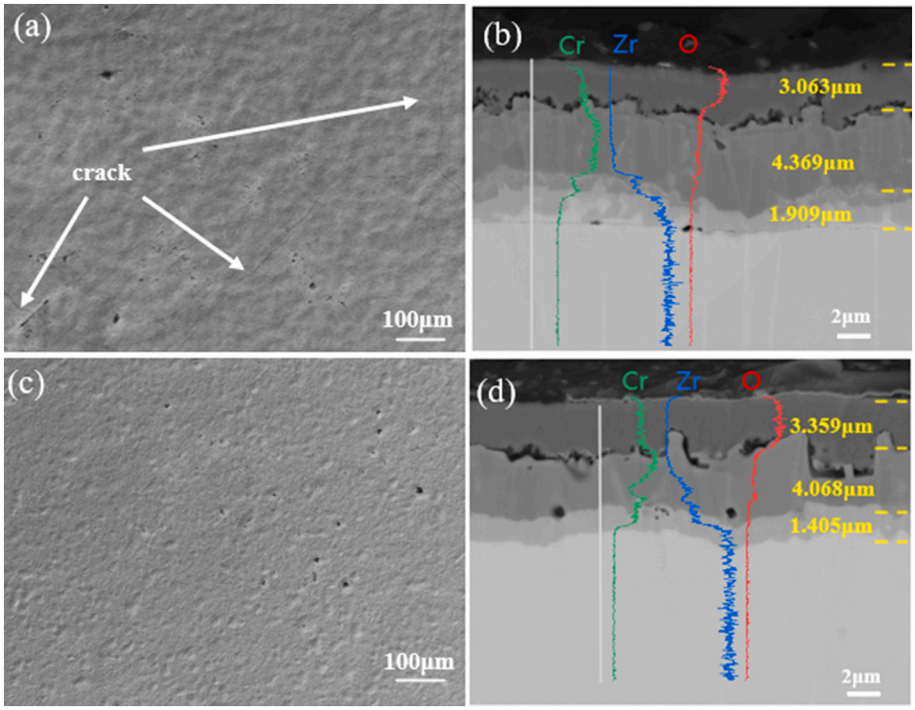

Fig. 12. Surface and cross-section SEM images of the Cr-coated ZIRLO substrates oxidized at 1200 °C for 90 min (a, b) HiPIMS without synchronized pulse bias (c, d) HiPIMS with synchronized pulse bias.

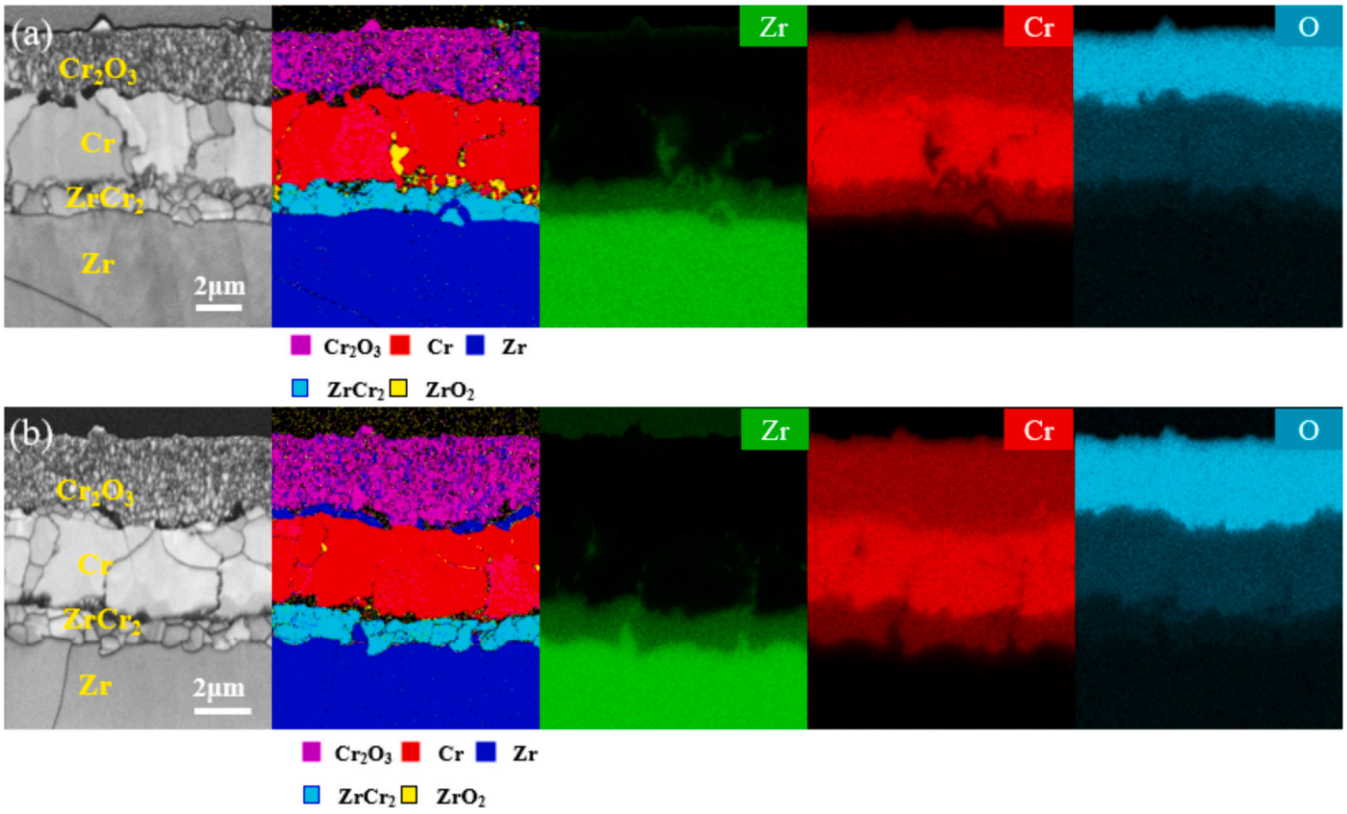

Fig. 13. EBSD plots and EDS plots of two coatings after steam oxidation at 1200 °C for 90 min (a) HiPIMS without synchronized pulse bias (b) HiPIMS with Synchronized pulse bias.

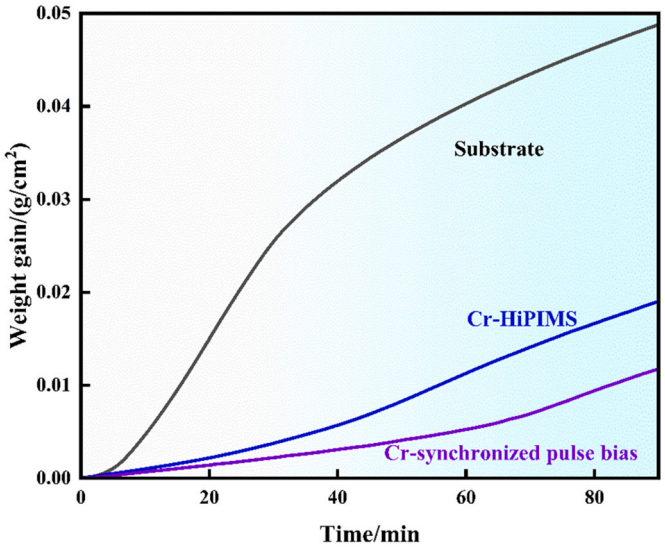

Fig. 14. Oxidation kinetics curves of the ZIRLO substrate and two kinds of Cr coatings in 1200 °C steam environment.

bias waveform and HiPIMS pulse discharge waveform of the sputtering cathode. This results in the selective energization of the sputtered material ions. Cr atoms with higher energy induce selective deposition of Cr ions in the (200) plane during the deposition process. Hence, compared with the Cr coatings prepared without synchronized pulse bias, the Cr coatings prepared with synchronized pulse bias possess obvious Cr (200) preferred orientation. In addition, because of the Cr atom with lower energy for the Cr coatings prepared without synchronized pulse bias, the difference of grains is significant, as shown in Fig. 4(b). With the use of synchronized pulse bias, the Cr atoms with higher energy induce the difference between grains becoming inconspicuous and compact small grains uniform formation on the surface of the Cr coatings prepared with synchronized pulse bias, as shown in Fig. 4(e). As depicted in Fig. 6(a), the employment of synchronized pulse bias introduces higher energy Cr atoms that disrupt the formation of columnar crystals, resulting in the deposition of a coating with a more compact and uniform structure.

In order to explore the 1200 °C high-temperature steam oxidation properties, the schematic of the Cr coatings prepared with and without synchronized pulse bias is shown in Fig. 15. In the initial stage, the Cr coatings prepared with synchronized pulse bias have smaller grains and more grain boundaries due to the synchronized pulse bias. These grain boundaries result in a Cr coating that is more susceptible to the reaction of steam to form Cr_2O_3. In addition, the Cr coatings prepared with synchronized pulse bias possess an obvious Cr (200) preferred orientation. Cr (200) preferred orientation with the highest surface energy, which facilitates the adsorption of oxygen atoms and their reaction with the Cr coating. With the exposure time prolonged, the Cr coatings prepared with synchronized pulse bias preferential react with steam and generate more compact Cr_2O_3 equiaxed crystals, which makes it difficult for steam to further diffuse into Cr layers. As a result, the initial oxidation weight gain per unit area is lower for Cr coatings prepared using synchronized pulse bias, as shown in Fig. 14. After 30 min of high-temperature steam oxidation, it was found that the grain size of the Cr coatings prepared with synchronized pulse bias was larger. It seems that this study is the same as the previous reports [41], which showed that the Cr coatings exhibited better oxidation resistance when they were in (200) preferred orientation and found that rapid grain growth was detected in (200) preferred orientation Cr coatings after a short period of high temperature. This phenomenon can be explained by the preferential growth of bcc material along ⟨100⟩. Given that grain boundaries can act as oxygen diffusion short paths in the oxidation process, which is also supported by the EBSD results (Fig. 9). During high-temperature steam

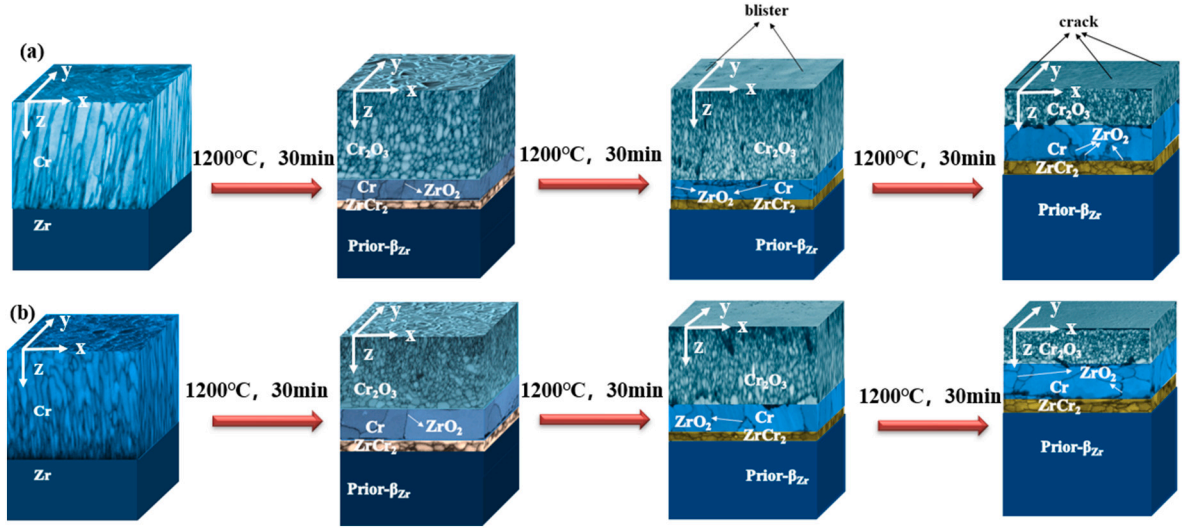

Fig. 15. Schematic diagram of the oxidation process of two coatings in a steam environment at 1200 °C (a) HiPIMS without synchronized pulse bias (b) HiPIMS with synchronized pulse bias.

oxidation, Zr diffuses upward along the grain boundaries of Cr and reacts with the downward diffusing oxygen to form ZrO_2 grains within the Cr grain boundaries. It has been demonstrated that the ZrO_2 grains present in the residual Cr layer play a significant role as the primary pathway for oxygen diffusion, which ultimately leads to the failure of the Cr coating [36]. The coarsened Cr grains with reduced grain boundary fraction in the residual coatings are suggested to contribute to the excellent steam oxidation resistance in the Cr coatings prepared with synchronized pulse bias.

When the high-temperature steam oxidation time was increased to 60 min, Cr coatings prepared with synchronized pulse bias showed a relatively flat surface. In contrast, numerous bubbles appeared on the surface of Cr coatings prepared without synchronized pulse bias. The formation of bubbles on the surface of the Cr coating can be attributed to the enhanced diffusion of steam into the Cr_2O_3 oxide layer. This leads to the generation of volatile compounds such as CrO_3 and $CrO_2(OH)_2$. The observation also revealed numerous pores within the Cr_2O_3 oxide layer and at the Cr/Cr_2O_3 interface in the Cr coatings prepared without synchronized pulse bias. The formation of pores in the Cr_2O_3 oxide layer is attributed to the evaporation of CrO_3 and $CrO_2(OH)_2$. As illustrated in Figs. 8, 10 and 12, the number of pores in the Cr_2O_3 oxide layer decreases with the increase in oxidation time. This phenomenon can be attributed to the fact that the generation of CrO_3 and $CrO_2(OH)_2$ occurs primarily during the initial stages of oxidation. In contrast, the pores on the Cr/Cr_2O_3 interface are the result of vacancy coalescence. During the oxidation process, the growth of Cr_2O_3 grains is mainly due to the outward diffusion of Cr^{3+} to the Cr_2O_3 grain/gas interface for grain growth. Consequently, the pores on Cr/Cr_2O_3 are due to the condensation of Cr vacancies after the outward diffusion of Cr^{3+}. The less dense Cr_2O_3 oxide layer of the Cr coating prepared without synchronized pulse bias allows for greater steam diffusion into the layer, resulting in an increased presence of pores within the Cr_2O_3 oxide layer. The Cr_2O_3 oxide density of the Cr coatings prepared without synchronized pulse bias is lower, leading to easier diffusion of Cr^{3+} outwards, resulting in more pores at the Cr/Cr_2O_3 interface. Despite increasing the oxidation time to 60 min, the thicknesses of the Cr layer and Cr_2O_3 oxide layer in both Cr coatings remained nearly unchanged compared to those observed at 30 min. According to previous literature [39], there is a significant reduction reaction of Cr_2O_3 in both Cr coatings. This reduction reaction is supported by the wavy Cr/Cr_2O_3 interface and swollen ZrO_2 grains.

Increasing the high temperature steam oxidation time to 90 min resulted in further diffusion of steam, leading to the appearance of numerous bubbles and cracks on the surface of Cr coatings prepared without synchronized pulse bias. In contrast, the surface of the Cr coatings prepared with synchronized pulse bias remained remarkably flat, free of bubbles and cracks. It is also evident that the Cr_2O_3 layer in both Cr coatings undergoes rapid depletion. This depletion is due to both the interaction with steam and the reduction reaction with Zr. Furthermore, it can be seen from Fig. 12(b) and (d) that the Cr layer thickness in the Cr coating prepared with synchronized pulse bias is smaller than that in the coating prepared without synchronized pulse bias, while the Cr_2O_3 layer thickness in the former is larger than that in the latter. These observations differ significantly from those made at 30 and 60 min. This phenomenon can be attributed to the presence of cracks and defects on the surface of the Cr_2O_3 layer prepared without synchronized pulse bias, which act as diffusion pathways for steam, thereby accelerating its diffusion into the Cr coating. In addition, larger ZrO_2 grains are present in the grain boundary of the Cr layer in the Cr coating prepared without synchronized pulse bias. This facilitates the outward diffusion of zirconium along the grain boundary of the Cr layer, greatly enhancing the reduction reaction between Cr_2O_3 and Zr [42]. This results in the thickening of the Cr layer and the thinning of the Cr_2O_3 layer. The flat and dense Cr_2O_3 layer on the surface of Cr coatings prepared by synchronized pulse bias impedes the inward diffusion of oxygen and restricts the formation of ZrO_2 grains. The results indicate a lack of ZrO_2 grains in the residual Cr layer of the synchronized pulse bias prepared Cr coatings, suggesting that the synchronized pulse bias prepared Cr coatings have better antioxidant properties. Therefore, as the exposure time increased, the Cr coating prepared with synchronized pulse bias showed a lower oxidation weight gain per unit area compared to the Cr coating prepared without synchronized pulse bias, as shown in Fig. 14. Thus, the pulsed synchronized pulse bias helps to enhance the (200) preferred orientation of the Cr coating and improves the resistance of the coating to high-temperature oxidation.

5. Conclusion

(1) Two methods of preparation, HiPIMS with and without synchronized pulse bias, were employed to deposit Cr coatings with a (200) preferred orientation on the zirconium alloys substrate surface. The synchronized pulse bias technique resulted in an obvious (200) preferred orientation of the Cr coatings.

(2) The steam oxidation resistance of the coatings was compared at a temperature of 1200 °C. The Cr coatings prepared with synchronized pulse bias demonstrated superior resistance to steam oxidation at high temperatures compared to the Cr coatings

prepared without synchronized pulse bias. This improvement can be attributed to the microstructure developed during high-temperature oxidation. The results indicate that the Cr coatings prepared with synchronized pulse bias exhibit a dense and smooth surface, interrupted columnar crystal growth, and preferential formation of a dense Cr_2O_3 layer during high-temperature oxidation. These characteristics play a crucial role in impeding the diffusion of external oxygen into the zirconium substrate.

(3) Due to the (200) preferred orientation of the Cr coatings prepared with synchronized pulse bias, the residual Cr layer of the Cr coatings prepared with synchronized pulse bias grows faster and has a larger grain size in high-temperature steam environments, which reduces the formation of diffusion channels of oxygen, such as ZrO_2, and maybe the reason for the superior oxidation resistance under high-temperature steam conditions.

CRediT authorship contribution statement

Zhichao Han: Writing – original draft, Methodology. **Zhenyu Wang:** Writing – review & editing, Data curation, Resources, Supervision. **Shiyao Tan:** Investigation. **Aiying Wang:** Supervision, Funding acquisition. **Zhongyu Piao:** Data curation, Resources, Writing – review & editing. **Peiling Ke:** Writing – review & editing, Funding acquisition.

Declaration of competing interest

The authors declare that they have no known competing financial interests or personal relationships that could have appeared to influence the work reported in this paper.

Data availability

Data will be made available on request.

Acknowledgements

This work was financially supported by the National Natural Science Foundation of China (U22A20111), Key Research and Development Program of Ningbo (2023Z110), Natural Science Foundation of Ningbo (2023QL049), and Youth Innovation Promotion Association CAS (2023312).

References

[1] W. Li, Z. Wang, J. Shuai, B. Xu, A. Wang, P. Ke, A high oxidation resistance Ti2AlC coating on Zirlo substrates for loss-of-coolant accident conditions, Ceram. Int. 45 (11) (2019) 13912–13922, https://doi.org/10.1016/j.ceramint.2019.04.089.

[2] K.A. Terrani, Accident tolerant fuel cladding development: promise, status, and challenges, J. Nucl. Mater. 501 (2018) 13–30, https://doi.org/10.1016/j.jnucmat.2017.12.043.

[3] T.M. Copeland-Johnson, C.K.A. Nyamekye, S.K. Gill, L. Ecker, N. Bowler, E. A. Smith, et al., Characterization of Kanthal APMT and T91 oxidation at beyond design-basis accident temperatures, Corros. Sci. 171 (2020), https://doi.org/10.1016/j.corsci.2020.108598.

[4] Y. Wang, Y. Yang, Study on containment pressure response with passive containment cooling system performance under design basis accident, Prog. Nucl. Energy 94 (2017) 22–35, https://doi.org/10.1016/j.pnucene.2016.10.002.

[5] C. Tang, M. Stueber, H.J. Seifert, M. Steinbrueck, Protective coatings on zirconium-based alloys as accident-tolerant fuel (ATF) claddings, Corros. Rev. 35 (3) (2017) 141–165, https://doi.org/10.1515/corrrev-2017-0010.

[6] Z. Wang, G. Ma, L. Liu, L. Wang, P. Ke, Q. Xue, et al., High-performance Cr2AlC MAX phase coatings: oxidation mechanisms in the 900–1100°C temperature range, Corros. Sci. 167 (2020), https://doi.org/10.1016/j.corsci.2020.108492.

[7] X. Han, Y. Wang, S. Peng, H. Zhang, Oxidation behavior of FeCrAl coated Zry-4 under high temperature steam environment, Corros. Sci. 149 (2019) 45–53, https://doi.org/10.1016/j.corsci.2019.01.004.

[8] J.-M. Kim, T.-H. Ha, J.-S. Park, H.-G. Kim, Effect of laser surface treatment on the corrosion behavior of FeCrAl-coated TZM alloy, Metals 6 (2) (2016), https://doi.org/10.3390/met6020029.

[9] Y. Al-Olayyan, G.E. Fuchs, R. Baney, J. Tulenko, The effect of Zircaloy-4 substrate surface condition on the adhesion strength and corrosion of SiC coatings, J. Nucl. Mater. 346 (2–3) (2005) 109–119, https://doi.org/10.1016/j.jnucmat.2005.05.016.

[10] X. Han, C. Chen, Y. Tan, W. Feng, S. Peng, H. Zhang, A systematic study of the oxidation behavior of Cr coatings on Zry4 substrates in high temperature steam environment, Corros. Sci. 174 (2020), https://doi.org/10.1016/j.corsci.2020.108826.

[11] Z. Wang, W. Li, Z. Wang, M. Li, A. Wang, P. Ke, Comparative study on protective Cr coatings on nuclear fuel cladding Zirlo substrates by AIP and HiPIMS techniques, Ceram. Int. 49 (14) (2023) 22736–22744, https://doi.org/10.1016/j.ceramint.2023.04.074.

[12] J. Yang, M. Steinbruck, C. Tang, M. Grosse, J. Liu, J. Zhang, et al., Review on chromium coated zirconium alloy accident tolerant fuel cladding, J. Alloys Compd. 895 (2022), https://doi.org/10.1016/j.jallcom.2021.162450.

[13] A. Fazi, K. Stiller, H.-O. Andrén, M. Thuvander, Cold sprayed Cr-coating on optimized ZIRLOTM claddings: the Cr/Zr interface and its microstructural and chemical evolution after autoclave corrosion testing, J. Nucl. Mater. 560 (2022), https://doi.org/10.1016/j.jnucmat.2022.153505.

[14] Q.S. Chen, C.H. Liu, R.Q. Zhang, H.Y. Yang, T.G. Wei, Y. Wang, et al., Microstructure and high-temperature steam oxidation properties of thick Cr coatings prepared by magnetron sputtering for accident tolerant fuel claddings: the role of bias in the deposition process, Corros. Sci. 165 (2020), https://doi.org/10.1016/j.corsci.2019.108378.

[15] Y. Xiang, H. Yang, Q. Chen, X. Peng, R. Zhang, T. Wei, et al., Long-term high-temperature steam oxidation behavior of Cr-coated Zircaloy-4 alloy for accident tolerant fuel, Mater. Corros. 73 (12) (2022) 2009–2018, https://doi.org/10.1002/maco.202213307.

[16] A. Liang, Y. Wang, F. Wang, L. Qiang, Fantastic behavior of near zero wear of Cr-based coatings, Mater. Lett. 319 (2022), https://doi.org/10.1016/j.matlet.2022.132228.

[17] D.J.M. King, S.T.Y. Cheung, S.A. Humphry-Baker, C. Parkin, A. Couet, M.B. Cortie, et al., High temperature, low neutron cross-section high-entropy alloys in the Nb-Ti-V-Zr system, Acta Mater. 166 (2019) 435–446, https://doi.org/10.1016/j.actamat.2019.01.006.

[18] C. Xiang, E.H. Han, Z.M. Zhang, H.M. Fu, J.Q. Wang, H.F. Zhang, et al., Design of single-phase high-entropy alloys composed of low thermal neutron absorption cross-section elements for nuclear power plant application, Intermetallics 104 (2019) 143–153, https://doi.org/10.1016/j.intermet.2018.11.001.

[19] M. Ševeček, A. Gurgen, A. Seshadri, Y. Che, M. Wagih, B. Phillips, et al., Development of Cr cold spray–coated fuel cladding with enhanced accident tolerance, Nucl. Eng. Technol. 50 (2) (2018) 229–236, https://doi.org/10.1016/j.net.2017.12.011.

[20] Y. Wang, W. Zhou, Q. Wen, X. Ruan, F. Luo, G. Bai, et al., Behavior of plasma sprayed Cr coatings and FeCrAl coatings on Zr fuel cladding under loss-of-coolant accident conditions, Surf. Coat. Technol. 344 (2018) 141–148, https://doi.org/10.1016/j.surfcoat.2018.03.016.

[21] H. Yeom, B. Maier, G. Johnson, T. Dabney, M. Lenling, K. Sridharan, High temperature oxidation and microstructural evolution of cold spray chromium coatings on Zircaloy-4 in steam environments, J. Nucl. Mater. 526 (2019), https://doi.org/10.1016/j.jnucmat.2019.151737.

[22] H.-G. Kim, I.-H. Kim, Y.-I. Jung, D.-J. Park, J.-Y. Park, Y.-H. Koo, Adhesion property and high-temperature oxidation behavior of Cr-coated Zircaloy-4 cladding tube prepared by 3D laser coating, J. Nucl. Mater. 465 (2015) 531–539, https://doi.org/10.1016/j.jnucmat.2015.06.030.

[23] T. Zhang, H. Liao, W. Huang, H. Ruan, Y. Su, X. Yang, et al., High temperature steam oxidation behavior of textured Cr coatings with different grain structures, Surf. Coat. Technol. 459 (2023), https://doi.org/10.1016/j.surfcoat.2023.129358.

[24] E.B. Kashkarov, D.V. Sidelev, N.S. Pushilina, J. Yang, C. Tang, M. Steinbrueck, Influence of coating parameters on oxidation behavior of Cr-coated zirconium alloy for accident tolerant fuel claddings, Corros. Sci. 203 (2022), https://doi.org/10.1016/j.corsci.2022.110359.

[25] Y. Meng, S. Zeng, C. Chen, C. Zhu, H. Shen, X. Zhou, et al., Effect of deposition parameters on characteristics and oxidation behavior of magnetron sputtered Cr coatings, J. Nucl. Mater. 588 (2024), https://doi.org/10.1016/j.jnucmat.2023.154802.

[26] X. He, Z. Tian, B. Shi, X. Xu, C. Meng, W. Dang, et al., Effect of gas pressure and bias potential on oxidation resistance of Cr coatings, Ann. Nucl. Energy 132 (2019) 243–248, https://doi.org/10.1016/j.anucene.2019.04.038.

[27] C.-C. Kuo, C.-H. Lin, Y.-T. Lin, J.-T. Chang, Effects of cathode voltage pulse width in high power impulse magnetron sputtering on the deposited chromium thin films, Coatings 10 (6) (2020), https://doi.org/10.3390/coatings10060542.

[28] D.N. Lee, A model for development of orientation of vapour deposits, J. Mater. Sci. 24 (12) (1989) 4375–4378, https://doi.org/10.1007/bf00544515.

[29] J.-M. Zhang, F. Ma, K.-W. Xu, Calculation of the surface energy of bcc metals by using the modified embedded-atom method, Surf. Interface Anal. 35 (8) (2003) 662–666, https://doi.org/10.1002/sia.1587.

[30] X. Wang, H. Guan, Y. Liao, M. Zhu, C. Xu, X. Jin, et al., Enhancement of high temperature steam oxidation resistance of Zr–1Nb alloy with ZrO2/Cr bilayer coating, Corros. Sci. 187 (2021), https://doi.org/10.1016/j.corsci.2021.109494.

[31] J.-C. Brachet, E. Rouesne, J. Ribis, T. Guilbert, S. Urvoy, G. Nony, et al., High temperature steam oxidation of chromium-coated zirconium-based alloys: kinetics and process, Corros. Sci. 167 (2020), https://doi.org/10.1016/j.corsci.2020.108537.

[32] W. Wang, G. Zhang, C. Wang, T. Wang, T. Li, Construction of chromium coatings with (200) preferred orientation and exploration the high-temperature steam oxidation properties, J. Nucl. Mater. 563 (2022), https://doi.org/10.1016/j.jnucmat.2022.153660.

[33] J. Wu, M. Shen, M. Hu, C. Guo, Q. Li, S. Zhu, High vacuum arc ion plating Cr films: self-ion bombarding effect and oxidation behavior, Corros. Sci. 187 (2021), https://doi.org/10.1016/j.corsci.2021.109476.
[34] M. Hu, M. Shen, Z. Liu, C. Guo, Q. Li, S. Zhu, Self-ion bombarded Cr films: crystallographic orientation and oxidation behaviour, Corros. Sci. 143 (2018) 212–220, https://doi.org/10.1016/j.corsci.2018.08.016.
[35] M. Steinbrück, U. Stegmaier, M. Große, L. Czerniak, E. Lahoda, R. Daum, et al., High-temperature oxidation and quenching of chromium-coated zirconium alloy ATF cladding tubes with and w/o pre-damage, J. Nucl. Mater. 559 (2022), https://doi.org/10.1016/j.jnucmat.2021.153470.
[36] X. Hu, C. Dong, Q. Wang, B. Chen, H. Yang, T. Wei, et al., High-temperature oxidation of thick Cr coating prepared by arc deposition for accident tolerant fuel claddings, J. Nucl. Mater. 519 (2019) 145–156, https://doi.org/10.1016/j.jnucmat.2019.01.039.
[37] T. Wei, R. Zhang, H. Yang, H. Liu, S. Qiu, Y. Wang, et al., Microstructure, corrosion resistance and oxidation behavior of Cr-coatings on Zircaloy-4 prepared by vacuum arc plasma deposition, Corros. Sci. 158 (2019), https://doi.org/10.1016/j.corsci.2019.06.029.
[38] J.K. Liu, Z.X. Cui, Z. Hao, D.Y. Ma, J.Q. Lu, Y.G. Cui, et al., Steam oxidation of Cr-coated Sn-containing Zircaloy solid rod at 1000 °C, Corros. Sci. 190 (2021), https://doi.org/10.1016/j.corsci.2021.109682.
[39] J. Liu, M. Steinbrueck, M. Grosse, U. Stegmaier, C. Tang, D. Yun, et al., Systematic investigations on the coating degradation mechanism during the steam oxidation of Cr-coated Zry-4 at 1200°C, Corros. Sci. 202 (2022), https://doi.org/10.1016/j.corsci.2022.110310.
[40] J.K. Liu, C.C. Tang, M. Steinbrück, J.Q. Yang, U. Stegmaier, M. Grosse, et al., Transient experiments on oxidation and degradation of Cr-coated Zircaloy in steam up to 1600 °C, Corros. Sci. 192 (2021), https://doi.org/10.1016/j.corsci.2021.109805.
[41] Y. Wang, L. Wang, L. Shang, G. Bai, J. Li, F. Xue, et al., Fiber texture-dependent oxidation behaviour of Cr-coated zirconium alloy in high temperature steam, Corros. Sci. 205 (2022), https://doi.org/10.1016/j.corsci.2022.110449.
[42] W. Wang, G. Zhang, C. Wang, T. Wang, Y. Zhang, T. Xin, Investigations on 1200 °C steam oxidation behavior of Cr coatings with distinct crystallographic orientation on Zircaloy-4 alloys, J. Nucl. Mater. 592 (2024), https://doi.org/10.1016/j.jnucmat.2024.154945.